© 2021. Published by The Company of Biologists Ltd | Journal of Experimental Biology (2021) 224, jeb236240. doi:10.1242/jeb.236240

RESEARCH ARTICLE

Wing damage affects flight kinematics but not flower tracking performance in hummingbird hawkmoths

Klara Kihlström[1], Brett Aiello[2,3], Eric Warrant[1], Simon Sponberg[2,3] and Anna Stöckl[1,4,*]

ABSTRACT

Wing integrity is crucial to the many insect species that spend distinct portions of their life in flight. How insects cope with the consequences of wing damage is therefore a central question when studying how robust flight performance is possible with such fragile chitinous wings. It has been shown in a variety of insect species that the loss in lift-force production resulting from wing damage is generally compensated by an increase in wing beat frequency rather than amplitude. The consequences of wing damage for flight performance, however, are less well understood, and vary considerably between species and behavioural tasks. One hypothesis reconciling the varying results is that wing damage might affect fast flight manoeuvres with high acceleration, but not slower ones. To test this hypothesis, we investigated the effect of wing damage on the manoeuvrability of hummingbird hawkmoths (*Macroglossum stellatarum*) tracking a motorised flower. This assay allowed us to sample a range of movements at different temporal frequencies, and thus assess whether wing damage affected faster or slower flight manoeuvres. We show that hummingbird hawkmoths compensate for the loss in lift force mainly by increasing wing beat amplitude, yet with a significant contribution of wing beat frequency. We did not observe any effects of wing damage on flight manoeuvrability at either high or low temporal frequencies.

KEY WORDS: Flight control, Flower tracking, *Macroglossum stellatarum*, Insect, Wing damage

INTRODUCTION

Insects are masters of flight – with their fragile chitinous wings they perform impressive aerobatic manoeuvres, such as a dragonfly catching its prey in the air, or a hawkmoth hover-feeding from a flower which is moving in the wind. Yet, wing wear caused by collisions or predation is almost unavoidable for most insect species. The consequences of wing damage on flight kinematics have been investigated in variety of insect species. A general trend across different insect groups is that a reduction in wing area, and consequently in lift force (Ellington, 1984a), is compensated for by an increase in wing beat frequency (bumblebees: Hedenström et al., 2001; Haas and Cartar, 2008; hawkmoths: Fernández et al., 2012; Fernández et al., 2017; butterflies: Kingsolver, 1999). Force production also scales with increased wing beat amplitude, which might therefore also compensate the loss in lift force (Ellington, 1984c). However, wing beat amplitude does not change in bumblebees with either symmetric or asymmetric wing damage (Hedenström et al., 2001), and only marginally upon asymmetric wing damage in the hawkmoth *Manduca sexta* (Fernández et al., 2012; Fernández et al., 2017). While these kinematic changes after wing damage increase the metabolic cost of hovering in hawkmoths (Fernández et al., 2017), they did not affect it in bumblebees (Hedenström et al., 2001). The increased mortality of bumblebees with damaged wings (Cartar, 1992) was therefore hypothesised to result from an impaired flight performance caused by wing damage in this species.

The effects of wing damage on flight performance across different insect species have been shown to vary considerably, depending on the species and flight task. No effects of wing damage on free flight activity or initial dispersal rates were observed in the Wester white butterfly (Kingsolver, 1999). Also in bumblebees, no significant changes in foraging performance, flight speed, acceleration or distance to the ground were observed upon artificially inflicted wing damage in a simple foraging task in bumblebees (Haas and Cartar, 2008). However, in a more complex foraging task, the bumblebee's peak acceleration during lateral manoeuvres was reduced, though their obstacle avoidance success remained intact (Mountcastle et al., 2016). A much more distinct impairment of manoeuvrability was found in wing-damaged dragonflies, where a clear decrease in vertical acceleration and average velocity was documented, in addition to a reduction in prey capture success, for which complex aerial manoeuvres are required (Combes et al., 2010). Thus, one might hypothesise that wing damage affects aerial manoeuvres with high-acceleration components stronger than steady flight or take-off and landing. This hypothesis is further supported by studies in vertebrate flyers: in two species of bat (*Myotis albescens* and *Myotis nigricans*), individuals with damaged wing membranes were able to maintain flight speed, but performed fewer manoeuvres in comparison to conspecifics with intact wings (Voigt, 2013). In line with these results, a comparative study on hummingbird wing shape found that species with lower wing load have enhanced manoeuvrability, in particular greater rotational speeds during manoeuvres (Dakin et al., 2018). Since insect wing damage will also cause an increase in wing loading, one might therefore predict a reduced degree of manoeuvrability.

We therefore decided to investigate the effect of wing damage on the manoeuvrability of a hawkmoth in a naturalistic foraging task. Hawkmoths provide a suitable study system as their hovering kinematics (including energy requirements with intact and damaged wings; Fernández et al., 2017) have been well described (Ellington and Lighthill, 1984a; Ellington, 1984a,b,c,b; Willmott and Ellington, 1997a,b), and their natural foraging mode of extracting nectar while hovering in front of flowers can be exploited to directly study the effects of changes in sensory inputs or kinematic parameters on their fast corrective lateral flight manoeuvres (Farina et al., 1994;

[1]Lund Vision Group, Department of Biology, Lund University, 22362 Lund, Sweden. [2]School of Physics, Georgia Institute of Technology, Atlanta, GA 30332, USA. [3]School of Biological Sciences, Georgia Institute of Technology, Atlanta, GA 30332, USA. [4]Behavioral Physiology and Sociobiology (Zoology II), University of Würzburg, 97074 Würzburg, Germany.

*Author for correspondence (anna.stoeckl@uni-wuerzburg.de)

K.K., 0000-0003-0613-9129; B.A., 0000-0001-9034-0460; E.W., 0000-0001-7480-7016; S.S., 0000-0003-4942-4894; A.S., 0000-0002-0833-9995

Received 24 August 2020; Accepted 13 January 2021

Journal of Experimental Biology (2021) 224, jeb236240. doi:10.1242/jeb.236240

Sprayberry and Daniel, 2007; Sponberg et al., 2015; Stöckl et al., 2017; Dahake et al., 2018). We focused our study on the diurnal hummingbird hawkmoth, *Macroglossum stellatarum*, which hibernates as an adult and therefore has a lifespan of several months (Pittaway, 1993), during which the risk of wing damage is not negligible. Using an artificial flower that was moved at a combination of different temporal frequencies (Fig. 1A), resulting in flower movements of a range of accelerations (Fig. 1C), we could directly probe whether wing damage affected flower tracking manoeuvres at any of these temporal frequencies. We expected effects of wing damage on flower tracking performance specifically at the higher temporal frequencies of flower movement that require rapid turning manoeuvres on the scale of a few wingstrokes, and correspondingly higher peak accelerations. Furthermore, comparing potential changes in flight kinematics upon wing damage in this small hawkmoth species with very high wingbeat frequencies reveals kinematic compensation strategies for wing damage across hawkmoths of different sizes and wing beat parameters.

MATERIALS AND METHODS

Animals

Wild adult *Macroglossum stellatarum* (Linnaeus 1758) (Sphingidae), were caught in Sorède, France. Eggs were collected and the caterpillars raised on their native host plant *Gallium* spp. The eclosed adults were allowed to fly and feed from artificial flowers similar to the experimental flowers, in flight cages (70 cm long, 60 cm wide, 50 cm high) in a 14 h:10 h light:dark cycle for at least 1 day before experiments.

Experimental groups

Three different experimental groups were tested: (1) control animals with intact wings, (2) animals with natural wing damage, which was caused by flying in their holding cages, and (3) animals with artificial wing damage (Fig. 1D, Tables 1 and 2) induced by cutting the distal tip of the forewing, following the shape of their hindwing for consistency to reach an average reduction of 19% in wing area and 25% in forewing length (the maximum amount of wing damage that would still allow the hawkmoths to take off). Since the natural wing damage was inflicted over time, the hawkmoths in this condition were a week older on average than hawkmoths in the other two conditions. Different hawkmoth individuals were tested in the three conditions. In total, we tested 17 animals in the control condition, 10 in the natural damage condition and 15 in the artificial damage condition. However, we only obtained body and wing morphology for 11 animals in the control condition, 8 in the natural damage condition and 15 in the artificial damage condition and analysed only this subset of animals for questions relating to body and wing morphology specifically.

We photographed every animal after the experiment and determined their body and wing size using Fiji software (Schindelin

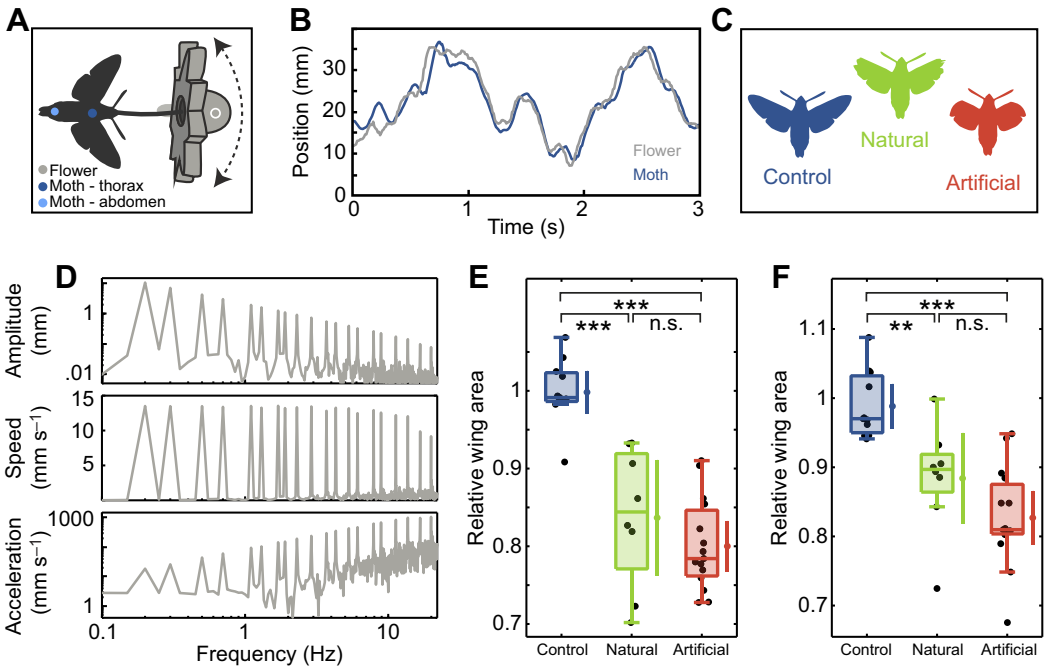

Fig. 1. The role of wing damage on hummingbird hawkmoth (*Macroglossum stellatarum*) flight performance. (A) We tested how wing damage affects hawkmoth flight performance in a naturalistic flight control task, using an artificial flower (48 mm diameter) that was attached to a stepper motor via a rod. To test the manoeuvrability of the animals, we moved the robotic flower while the animals were hover-feeding from the nectary, and thus attempted to track the flower to continue feeding. (B) Example flower and hawkmoth (thorax) positions in the axis of flower movement during a 3 s (out of a total of 20 s) stimulus sequence. (C) To study the effect of wing damage on flight and flower tracking performance, we compared a control group with intact wings (n=11) to a group with natural wing damage (n=8) and an artificial damage group (n=15) in which we clipped the distal forewings to the maximum extent possible that allowed the animals to fly. (D) The flower was moved using a superposition of sine-wave stimuli comprising different temporal frequencies. The amplitudes of flower movements (top panel) were adjusted to keep the velocity (middle panel) at the different frequencies constant, which resulted in an increase of flower acceleration with temporal movement frequency (bottom panel). (E,F) Forewing length and forewing area were normalised by the expected forewing length and area given each animal's body length (see Materials and Methods; Fig. S1D,E). Black dots denote individual hawkmoths, boxplots depict the median and 25th and 75th percentiles of the samples. Whiskers represent the data range excluding outliers (values extending 1.5 interquartile ranges beyond the upper and lower box limits). Statistical differences between groups are indicated as: ***P<0.001, **P<0.01, n.s. P>0.05 (ANOVA with Tukey's HSD corrected *post hoc* test was performed after testing the normality of residuals; Table S1). The coloured dot to the right of each boxplot shows the mean, and the bar indicates the 95% confidence interval.

Journal of Experimental Biology (2021) 224, jeb236240. doi:10.1242/jeb.236240

Table 1. Median and interquartile ranges for the measured morphological and kinematic features of control and wing damaged hummingbird hawkmoths

	Animal length (mm)	Wing length (mm)	Wing area (mm^2)	Wing beat frequency (Hz)	Projected amplitude (deg)	Stroke-plane amplitude (deg)
Control	31.0±4.6 *n*=11	23.7±3.1 *n*=11	135.3±42.7 *n*=11	75.9±8.2 *n*=17	78.3±16.6 *n*=17	86.6±16.9 *n*=17
Natural	28.2±2.0 *n*=8	19.9±3.1 *n*=8	109.4±26.2 *n*=8	79.9±7.2 *n*=10	91.2±21.8 *n*=10	99.6±21.3 *n*=10
Artificial	27.7±3.2 *n*=15	17.8±2.6 *n*=15	94.4±17.9 *n*=15	84.0±6.6 *n*=15	109.4±18.1 *n*=15	117.1±17.1 *n*=15

The projected wing beat amplitude was measured in the dorsal camera projection; the wing beat amplitude was transformed into the stroke plane with a stroke plane angle of 30.21 deg.

et al., 2012). Their total body length was measured along their anterior to posterior extent, the total wing length was measured for both wings, from the wing joint to the tip of their forewing, and the area of both wings was quantified by tracing with the polygon tool in Fiji. The data from the left and right wing was averaged for further analysis.

When reporting wing damage, we accounted for the individual size of the animals – and thus the individual size of their intact wings – by normalising the measured wing morphology of the three treatment groups with respect to the intact wing morphology expected for an animal of this size. This was possible because wing length and wing area scaled tightly with animal length (Pearson correlation coefficient r=0.94, r=0.95 and P<0.001, P<0.001, n=31, respectively; Fig. S1D, E). We therefore computed the allometric scaling between wing length (Fig. S1D) and wing area (Fig. S1E) using animals with intact wings (the control animals in this study, as well as an additional 20 animals with intact wings that were not tested with the robotic flower). To obtain the scaling exponent b and the scaling constant a of the allometric relationship:

$$y = ax^b, \quad (1)$$

we used Model II (reduced major axis) regression implemented in the gmregress script for MATLAB (A. Trujillo-Ortiz; https://www.mathworks.com/matlabcentral/fileexchange/27918-gmregress, retrieved March 19, 2020) to fit the parameters in the log-transformed version of the equation:

$$\log(y) = \log(a) + b\log(x). \quad (2)$$

This yields the scaling exponent b as the slope of the linear relationship, and the log-transformed scaling constant a as the y-axis intercept (Warton et al., 2006). With b=0.831 and a=1.397 for wing length, and b=1.831 and a=0.262 for wing area, we could use animal size to calculate the wing length and area that would be expected for the individuals in all treatment groups given their body length. These expected values were then used to normalise the measured wing length and area (Fig. 1E,F), so they represent the proportion of expected wing length and area for an animal of a given body length.

Table 2. Ratio of left divided by right wing length and area of hawkmoths in the different experimental conditions

		Control	Natural	Artificial
Wing length (R/L)	Mean±95% CI	1.004±0.009	1.004±0.029	1.016±0.026
	Median±IQR	1.007±0.014	1.007±0.045	1.004±0.067
Wing length (R/L)	Mean±95% CI	0.997±0.040	0.953±0.040	1.013±0.074
	Median±IQR	1.000±0.112	0.938±0.073	0.998±0.205
		n=10	*n*=8	*n*=15

Mean and 95% confidence interval, as well as median and inter-quartile-range (IQR) are shown. Since the mean and median differed distinctly from 1 for the wing length ratio in the natural condition, we tested whether the median differed significantly from 1 (Wilcoxon signed rank test, as data was not normally distributed: P=0.0547, signed rank=4).

Experimental setup

We used a robotic flower assay as our experimental setup. This assay was pioneered by Farina et al. (1994) and Sponberg et al. (2015), and also used in Roth et al. (2016), Stöckl et al. (2017) and Dahake et al. (2018). A flight cage of the same size as the holding cage was lined with soft muslin cloth and covered with black cloth on the three sides, while the front and top were sealed with Perspex plates for filming. A 3D-printed plastic flower (48 mm in diameter, on a 140 mm stalk) was placed at the centre of the flight cage. Placed at its centre was a nectary with an 8.3 mm opening, which was filled with 10% sucrose solution. The flower could be moved sideways in shallow arcs around the central pole, such that the primary motion was a lateral translation (Fig. 1A). The movement was controlled by a stepper motor (0.9 deg per step resolution, 1/16 microstepping, Phidgets, Inc.) and a custom-written MATLAB program. The cage was illuminated from above with an adjustable white LED panel and diffuser (CN-126 LED video light, Neewer). The light intensity was set to 3000 lx (measured with a ScreenMaster, B. Hagner AB, Solna, Sweden, at the position of the artificial flower). In addition, two 850 nm IR LED lights (LEDLB-16-IR-F, Larson Electronics) provided illumination for the infrared-sensitive high-speed video cameras (MotionBLITZ EoSens mini, Mikrotron), which were used to film the experiment. Videos were recorded at 100 fps, allowing us to record sequences of up to 28 s to analyse flower tracking.

Behavioural experiments

Individual moths were taken from their holding cage and introduced into the experimental cage. Animals in the artificial damage group were allowed to recover from cutting their wings for 24 h in the holding cage before participating in experiments. In the experimental cage, the hawkmoths were given 5 min to warm up their flight muscles and take flight. Most hawkmoths would approach the artificial flower within a few minutes after taking off. When their proboscis contacted the nectary, we started moving the artificial flower. If the animals did not take flight or did not feed from the flower within 10 min of taking off, we aborted the experiment and tested them again the next day. This way, we collected one complete 20 s flight-track from one individual per condition. To move the artificial flower, we used a 'sum-of-sines' stimulus of 20 s duration comprising a pseudo-random sum-of-sine stimulus composed of 20 temporal frequencies, which were prime multiples of each other to avoid harmonic overlap: 0.2, 0.3, 0.5, 0.7, 1.1, 1.3, 1.7, 1.9, 2.3, 2.9, 3.7, 4.3, 5.3, 6.1, 7.9, 8.9, 11.3, 13.7, 16.7, 19.9 Hz. High frequencies had lower amplitudes and vice versa, to assure equal peak velocities at all frequencies and avoid saturation due to power limitations (Roth et al., 2014) (Fig. 1C). This resulted in a range of movement distances from 11 mm at 0.2 Hz to 0.07 mm at 19.9 Hz, while the movement speed of the flower remained constant at around 13 mm s^{-1} up to 8.9 Hz, and dropped to 9 mm s^{-1} at the highest frequency owing to constraints of the motor. The acceleration of the stimulus scaled with the increase in temporal frequency, beginning at 16.5 mm s^{-2} at 0.2 Hz and rising up to 1000 mm s^{-2} for the three highest temporal frequencies.

Journal of Experimental Biology (2021) 224, jeb236240. doi:10.1242/jeb.236240

Flower tracking analysis

The positions of the flower and the hawkmoth were digitised from the videos using the DLTdv5 software for MATLAB (Hedrick, 2008) as described in Sponberg et al. (2015) and Stöckl et al. (2017). In brief, a marker on top of the flower and a reliably identifiable point on the thorax of the moth were used for reference for semi-automatic tracking. Tracking results were corrected manually using the same software where necessary. We only analysed sequences where the hawkmoth's proboscis was in contact with the nectary. To analyse changes in body pitch angle, we also tracked the tip of the abdomen for the first 200 frames of the stimulus, using manual tracking because the abdomen did not provide any reliable landmarks for automatic tracking. In the dorsal camera view, an increase in body pitch angle should manifest as a decrease in the distance between the thorax and abdomen tip (Fig. S3). We could not track the tip of the abdomen reliably in all videos, thus the number of individuals for this analysis was 14 in the control, 9 in the natural damage group and 10 in the artificial damage group.

To analyse the tracking performance across the entire stimulus, we extracted the absolute Euclidian distance between the hawkmoth's thorax and the nectary of the flower to obtain a measure for the displacement of hawkmoth and nectary. We calculated both the average displacement (as the median of distances across the entire stimulus duration), and the peak displacement (the 90% quantile of distances across the stimulus), to assess whether hawkmoths differ in their average tracking performance, or whether wing damage might produce specific tracking impairments that are not visible across the average (Fig. 5A,B). Moreover, we calculated the absolute length of the path the hawkmoth's thorax travelled, relative to the path length of the flower (Fig. 5B). To analyse the tracking performance at each temporal frequency of the stimulus, we extracted the amplitude and phase components in the corresponding power spectra at the stimulus frequencies. As in previous studies with the same stimulus (Sponberg et al., 2015; Stöckl et al., 2017), we did not analyse data at the highest two temporal frequencies (16.7, 19.9 Hz), because moths did not reliably track these frequencies. We used a system identification analysis (Cowan et al., 2014) to characterise the flower tracking performance of the hawkmoths as described previously (Sponberg et al., 2015; Stöckl et al., 2017). In brief, the tracking performance can be described by two components: gain and phase (Farina et al., 1994; Sponberg et al., 2015). The gain is the ratio of the amplitude of the hawkmoth's movement at the frequency relative to the flower's movement and would be 1 for perfect tracking. The phase is the amount that the hawkmoth leads or lags the flower movement measured in cycles of oscillations (deg) and would be 0 for perfect tracking. Since both gain and phase affect the positional error, and they are not independent, we used the tracking error ε metric (Roth et al., 2011; Sponberg et al., 2015), which incorporates effects of both gain and phase to quantify a straightforward-to-interpret tracking performance metric for our hawkmoths. It is calculated as the distance between the moth's response $H(s)$ and the ideal tracking conditions (gain=1, phase lag=0) in the complex plane, where s is the Laplace frequency variable:

$$\varepsilon(s) = H(s) - (1 + 0i). \quad (3)$$

A tracking error of 0, comprising a gain of 1 and a phase lag of 0, denotes perfect tracking, while at a tracking error larger than 1, the hawkmoths would produce better tracking results when remaining stationary. Because the tracking error metric is represented in the complex plane, we calculated the average of individual tracking errors and their confidence intervals by averaging data in the complex plane to avoid artefacts. These could arise from separating gain and phase components when transforming them and averaging in the non-complex plane (see Stöckl et al., 2017 for discussion). The 95% confidence intervals for gain and phase were calculated in the complex plane as in Stöckl et al. (2017).

The individual frequencies used in the analyses are not independent measures and instead represent part of dynamic systems characterization of the moth's response to the flower. Statistical tests are still being developed to compare frequency responses, because it is not clear how to combine data across frequencies. Lacking these, we took the approach of prior studies, which compare the 95% confidence intervals in the gain and phase plots and statistically compare the tracking error and other measures across specific frequency bands. To compare the tracking error across conditions, we pooled the data into two frequency ranges: high and low frequencies, as determined by the frequency range of natural flower movement, which concentrates 95% of total power in frequencies up to 1.7 Hz (as used for other hawkmoth species: Sponberg et al., 2015). We used this frequency as the limit for our

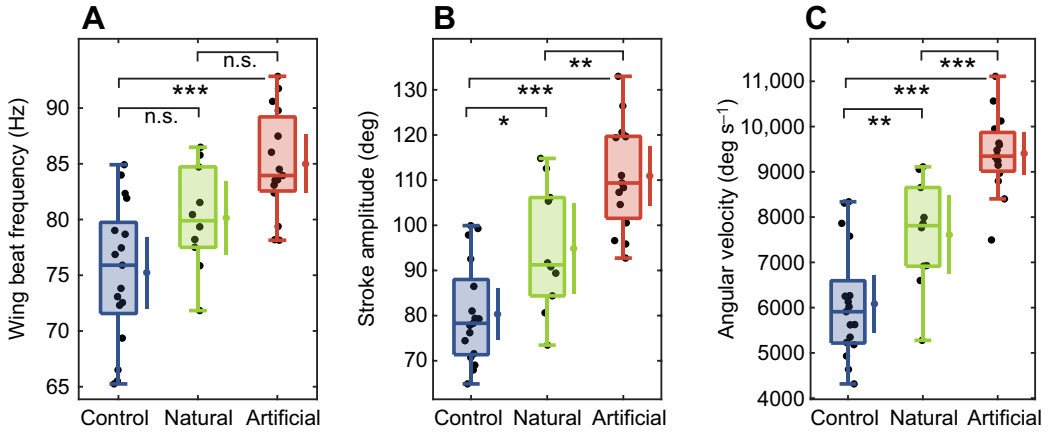

Fig. 2. Wing beat parameters were affected by wing damage in hummingbird hawkmoths. (A) Wing beat frequency and (B) horizontal projection of wing stroke amplitude measured during a hovering at the flower stimulus in control moths with no wing damage, and in moths with natural or artificially damaged wings. (C) Wing stroke velocity was calculated as the product of wing beat frequency and amplitude. Statistical differences between groups are indicated as: ***P<0.001, **P<0.01, *P<0.05, n.s. P>0.05 (ANOVA with Tukey's HSD corrected *post hoc* test was performed after confirming normality of residuals; Table S1; control: n=17; natural: n=10; artificial: n=15). The coloured dot to the right of each boxplot shows the mean, and the bar indicates the 95% confidence interval.

Journal of Experimental Biology

low frequency category (Fig. 6D), and frequencies higher than 1.7 Hz and up to and including 8.9 Hz into the high frequency range (Fig. 6E). We chose 8.9 Hz as the cut-off for comparability with previous studies on *Macroglossum stellatarum* (Stöckl et al., 2017; Dahake et al., 2018).

Wing kinematic analysis

To extract the wing beat frequency, as well as the amplitude of wing movement, we analysed the movement of the left wing tip for the first 100 frames of flower tracking. We thereby ensured that we analysed the same stimulus window for all moths to avoid biasing our results by analysing different flight manoeuvres caused by different sections of the stimulus. From these measurements, we extracted the wing beat frequency as the peak in the Fourier transformed wing tip position (Fig. S2A,B). Because we filmed at a frame rate of 100 fps, the animal's wing beat frequency was higher than the Nyquist sampling limit, which we corrected by subtracting the measured frequency from 100 Hz to obtain the actual wing beat frequency. We confirmed this wing beat frequency by filming 3 animals during stationary hovering at 600 fps (wing beat frequencies of these animals: 86.4, 78.4, 77.2 Hz; Fig. S2C,D). We could not film the tracking videos at 600 fps for all experiments because the memory limits of the camera did not allow sufficiently long videos for the frequency domain analysis. Thus, while our sampling rate was sufficient to quantify general changes in flight kinematics averaged over several consecutive wing strokes, we lacked the temporal resolution to resolve wingstroke by wingstroke adjustments.

We used Fiji to extract a horizontal projection of the wing stroke amplitude (Schindelin et al., 2012), measured as the angle between the two most extreme wing positions for each consecutive 10 wing beat sequence over an average of 100 wing beats in total. This resulted in 10 wing beat amplitude measurements per animal, which were then averaged to obtain the wing beat amplitude of the animal (Fig. S2E,F). This method ensured that we selected the maximum range of wing positions despite the frame rate undersampling of the wing beat frequency. We confirmed the accuracy of our amplitude analysis by comparing the results to the wing beat angles obtained in the brief, 600 fps control videos. With our dorsal camera view, we could not measure the wing stroke amplitude along the wing stroke plane, but measured a horizontal projection of it. Thus, changes in wing stroke angle might appear as changes in the projection amplitude we measured, as the actual wing stroke also extends into the vertical axis (Willmott and Ellington, 1997a). However, based on unpublished measurements of the wing stroke plane relative to the horizontal plane of *M. stellatarum*, which averages 30.21±3.8 deg interquartile range (IQR), the projection captures the majority of wing stroke amplitude change, and the method is consistent with approaches in other insect studies.

Aerodynamic model

We used established models of hovering flight (Ellington, 1984a,c; Fernández et al., 2017) to estimate the effects of wing damage on the lift force and mechanical power required for flapping the wings. We modelled the lift production and required mechanical power during flapping hovering for each individual. Following the methods of Fernández et al. (2017) and Ellington (1984c) lift production was modelled as:

$$L = \frac{1}{8}\rho S_2 n^2 \Phi^2 \overline{C_l}\overline{\left(\mathrm{d}\hat{\phi}/\mathrm{d}\hat{t}\right)^2}, \quad (4)$$

where ρ is air density, S_2 is the second moment of wing area, n is the wing beat frequency, Φ is wing beat amplitude, $\overline{C_l}$ is the average coefficient of lift, and $\overline{\left(\mathrm{d}\hat{\phi}/\mathrm{d}\hat{t}\right)^2}$ is the average square of the non-dimensional angular velocity. The required mechanical power was modelled as:

$$P_{\mathrm{mech}} = \frac{1}{16}\rho S_3 n^3 \Phi^3 \overline{C_\mathrm{d}}\overline{\left|\left(\mathrm{d}\hat{\phi}/\mathrm{d}\hat{t}\right)\right|^3}, \quad (5)$$

where S_3 is the third moment of wing area, $\overline{C_\mathrm{d}}$ is the average coefficient of drag, and $\overline{\left|\left(\mathrm{d}\hat{\phi}/\mathrm{d}\hat{t}\right)\right|^3}$ is the average of the absolute value of the cube of the non-dimensional angular velocity. Numerical values of $\overline{C_l}$, $\overline{C_\mathrm{d}}$, $\overline{\left(\mathrm{d}\hat{\phi}/\mathrm{d}\hat{t}\right)^2}$, and $\overline{\left|\left(\mathrm{d}\hat{\phi}/\mathrm{d}\hat{t}\right)\right|^3}$ were obtained from Fernández et al. (2017) and equal to 1.4, 1.6, 19.74, and 105.29, respectively. The coefficients of lift and drag for a given wing planform average a range of parameters as a function of the wing angle of attack. Average coefficients of the same value have been applied to wings ranging in shape from that of a fruit fly to that of a hummingbird (Hedrick et al., 2009). The assumption that many different wing shapes have similar force coefficients is supported by comparisons of force coefficients across a range of wing shapes (Usherwood and Ellington, 2002).

Since in these equations, the wing stroke amplitude Φ denotes the angular amplitude of the wing stroke in the wing stroke plane, rather than in the horizontal projection as we measured in our setup, and the transformation of the wing stroke angle from projection to stroke plane is not a linear one, we transformed the projected wing stroke angles into the wing stroke plane using the following transformation:

$$\Phi = 2{*}\arctan\left(\frac{\tan(\Phi_{\mathrm{proj}}/2)}{\cos(\beta)}\right), \quad (6)$$

where β denotes the angle between the horizontal plane and the wing stroke plane, and Φ_{proj} is the wing stroke amplitude measured in the horizontal projection. To calculate wing stroke amplitudes back to the horizontal projection for better comparison with our measured results, we used the relationships in Eqn 6.

To investigate the relative effect of modulating stroke amplitude and frequency to compensate for the loss in lift production upon wing damage, we calculated the necessary modulation required in either wing beat frequency or stroke amplitude, if the other variable remained at the average of an animal with intact wings. In other words, how much greater would the increase in wing beat frequency need to be if stroke amplitude was not modulated (and vice versa). To do this, the lift force was calculated for each individual in the artificial damage and natural damage group. Using the calculated lift, the equation was rearranged, the mean wing beat frequency from the control group was used to replace the wing beat frequency of that individual, and the resultant magnitude of the wing stroke amplitude was calculated. This procedure was then repeated while using the wing stroke amplitude of the mean control group to determine the wing beat frequency necessary to compensate lift for that individual.

To obtain the required second and third moments of wing area, wing morphology from the photographs of each moth was digitized using the StereoMorph package (v.1.6.2; https://cran.r-project.org/web/packages/StereoMorph/index.html) in R (v.3.4.2; https://www.r-project.org/). The rostral and caudal bases of the left and right forewing were digitized and a series of third order Bézier curves were used to outline each forewing. The curves of each wing were then resampled using the StereoMorph package to generate 50 evenly spaced points (semilandmarks) around the perimeter of each forewing.

The digital shape outputs of the left and right forewing from each moth were further analysed in MATLAB. First, each forewing was rotated so its long axis was perpendicular to the long axis of the body. Wing length, R, was measured as the distance between the minimum and maximum value of the wing outline. Wing area was calculated using the 'polyarea' function in MATLAB. For each wing, the second and third moments of area were calculated following Ellington (1984a).

RESULTS

We investigated the effects of wing damage on the hawkmoth *M. stellatarum* in three treatments: a control group with intact wings, a group with 'natural' wing damage that occurred in our flight cages, and an artificial damaged group, in which we trimmed the distal forewings to the maximum extent with which the animals were still able to fly (Fig. 1D). The natural damage group contained individuals with a wide range of wing damage, thus resulting in the widest spread of forewing area and forewing length of the three treatments (Fig. S1B,C, Table 1). We therefore normalised forewing length and forewing area relative to the expected length and size given an individual's body length (see Materials and Methods). Relative forewing length and area differed significantly between the damage treatments and the control group (ANOVA: F_2=34.04, P<0.001, Tukey's HSD corrected post-hoc test: P<0.001 for both comparisons), but not between artificial and natural damage (Tukey's HSD corrected *post hoc* test: P<0.381; Fig. 1E,F, Table 1 and Table S1): animals in the natural damage group had less than 84.4±14.8% of the wing length and 78.4±8.5% of the wing area of an intact animal, while the artificial group had 89.7±5.5% of wing length and 81.0±7.2% of wing area. Here, spread is reported as interquartile range if not indicated otherwise.

Wing beat kinematics during hovering flight

To analyse their wing beat kinematics, we filmed individual hawkmoths dorsally as they were hovering at the artificial flower (Fig. 1E,F). The wing beat frequency of the artificial damage group was significantly increased to 84.0±6.6 Hz compared with the control group at 75.9±8.2 Hz (ANOVA: F_2=13.09, P<0.001, Tukey's HSD corrected *post hoc* test: P<0.001, respectively; Fig. 2A, Table 1 and Table S1). The natural damage group had a median wing beat frequency intermediate of the other two groups, though it did not significantly differ from either the artificial damage or the control group (Tukey's HSD corrected *post hoc* test: P=0.083, P=0.070, respectively). Similarly, the horizontal projection of the wing stroke amplitude, measured as the angle between the maximum forward and backward extent of the forewing edge in the dorsal camera view, was significantly increased in the two damage groups compared with the control (ANOVA: F_2=25.35, P<0.001, Tukey's HSD corrected *post hoc* test: P=0.013, P<0.001; Fig. 2B). Moreover, it was significantly higher in the artificial group than the natural damage group (Tukey's HSD corrected *post hoc* test: P=0.007). In combination, the increased wing beat frequency and amplitude in the damaged groups resulted in a significantly higher wing beat velocity in the natural and artificial damage groups compared with the control (ANOVA: F_2=35.59, P<0.001, Tukey's HSD corrected *post hoc* test: P=0.004, P<0.001; Fig. 2C).

Since the relative wing length and wing area varied both across and also within treatment groups (Fig. 1D,E), we tested for correlations between wing anatomy and wing beat parameters across treatment groups. We observed a significant linear correlation between relative forewing length and wing beat frequency, wing beat amplitude and wing beat velocity (Fig. 3A–C; Pearson correlation coefficient r=−0.56, −0.64, −0.70 and P=0.001, P<0.001, P<0.001 for frequency, amplitude and velocity; n=34). Similarly, all wing beat parameters correlated significantly with the relative wing area (Fig. 3D–F; Pearson correlation coefficient r=−0.48, −0.61, −0.65 and P=0.004, P<0.001, P<0.001 for frequency, amplitude and velocity; n=34), although the variation explained was slightly lower.

To test whether there were treatment specific effects of wing anatomy on wing kinematics, we performed an analysis of covariance. We only found a significant interaction between wing anatomy and treatments for wing beat frequency and wing length (ANCOVA, group*winglength: F_2=4.4, P=0.022, resulting in a significant difference in slope between the control and the other two conditions: P=0.017 and intercept: P=0.026, but not between the natural and artificial damage group). None of the other comparisons yielded statistically significant interaction terms.

We also observed a change in the body pitch angle between treatments, measured as the distance between the thorax and the distal tip of the abdomen in the dorsal camera view. Hawkmoths in the artificial showed a steeper body pitch angle than animals in the control group (Fig. S3A; ANOVA: F_2=4.1, P=0.027, Tukey's HSD corrected *post hoc* test: P=0.021; Table S1), though there was no significant difference between the control and natural, and the artificial and natural groups (Table S1).

The effect of wing beat kinematics on lift and mechanical power

To test whether the increase in wing beat amplitude and frequency in the damage groups could compensate for the loss in lift force due to the reduced wing area, we calculated the effects of these parameters on the lift force and mechanical power required for flapping the wings (see Materials and Methods 'Aerodynamic model'). There was no significant difference in the estimated lift force across treatments (ANOVA: F_2=0.103, P=0.903; Fig. 4A, Table S1), indicating that the changes in wing beat amplitude and frequency observed in the damage treatment groups were sufficient to compensate for the loss in lift force due to the reduction in wing area. There was no significant difference between treatments in the mechanical power based on the measured wing area and wing beat kinematics (ANOVA: F_2=0.016, P=0.984; Fig. 4B, Table S1).

To determine if wing beat frequency or wing stroke amplitude contributed more strongly to lift compensation, we replaced the measured wing beat parameters by the median frequency and amplitude of the control group. Without any compensation, the loss of lift force was substantial: the median lift force in the natural damage group decreased significantly to 66.4±15.2% of the lift force generated with their measured wing beat parameters (Wilcoxon signed rank test: W_7=40, P=0.008), and in the artificial damage group to 50.0±8.5% (Wilcoxon signed rank test: W_{14}=0, P<0.001; Fig. 4C, Table S2B). Wing beat amplitude contributed more strongly to lift compensation than wing beat frequency in the artificial damage group, since the reduction upon fixing wing beat frequency to control values led to a significantly higher lift force than when the amplitude was fixed, which did not differ significantly from fixing both parameters (Fig. 4C; ANOVA: F_2=36.3, P<0.001, Tukey's HSD corrected *post hoc* test: P<0.001, P=0.007; Table S2A). However, both wing beat parameters contributed significantly to lift compensation, as the resulting lift forces with either one fixed were significantly reduced (Wilcoxon signed rank test, either frequency or amplitude fixed: W_{14}=0, P<0.001; Table S2B). A similar overall trend emerged for the natural damage treatment, although the lift force upon fixing wing beat amplitude was only marginally different from fixing wing beat frequency (ANOVA: F_2=6.9, P=0.005,

Journal of Experimental Biology (2021) 224, jeb236240. doi:10.1242/jeb.236240

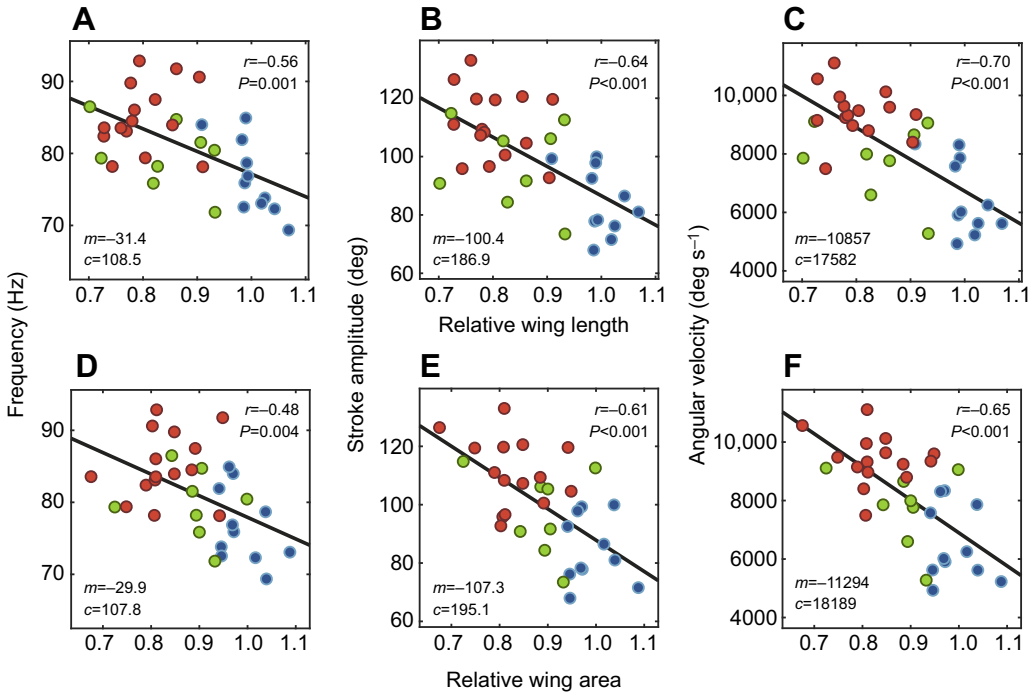

Fig. 3. Linear relationship between wing beat kinematics and wing anatomy. Ordinary least square regression of wing beat frequency (A,D), horizontal projection of wing stroke amplitude (B,E) and wing beat velocity (C,F) with the relative forewing length (A–C) and area (D–F). The strength of the linear correlation is given by *r*, and the statistical significance of the Pearson correlation coefficient by *P*. The model for the linear fit with slope *m* and intercept *c* is given in each panel (control: n=11; natural: n=8; artificial: n=15), the units of these parameters are the same as the *y*-axis units.

Tukey's HSD corrected *post hoc* test: P=0.07; Table S2A, Fig. 4C). Because of the proportional scaling of the lift force and mechanical power equations (Eqns 4 and 5), the effects of fixing wing beat amplitude and frequency on the resulting mechanical power were similar to those on the lift force generation (Fig. 4D).

To investigate the contribution of the two wing beat variables further, we calculated the modulation required in each variable to compensate lift force production if the other variable was fixed at the control group average. In other words, we calculated how much greater the increase in wing beat frequency would need to be if stroke amplitude was not modulated (and vice versa). It is important to note that the stroke amplitude in our model was assumed in the wing stroke plane, rather than in the horizontal projection as measured in our experiments. We therefore transferred the projected amplitudes to the stroke plane using an average stroke plane angle of 30.2 deg (see Materials and Methods). If stroke amplitude was fixed, the average wing beat frequency required to compensate lift force production was 92.6±10.3 Hz for the natural damage and 107.8±8.0 Hz for the artificial damage group, both significantly increased compared with the control (ANOVA: F_2=27.05, P<0.001, Tukey's HSD corrected *post hoc* test: P=0.004, P<0.001; Fig. 4E, Table S1). When wing beat frequency was fixed, the average wing beat amplitude required to compensate lift force production was 111.9±12.5 deg for natural damaged wings and 130.3±9.6 deg for artificial damaged wings, both significantly different from the control group (ANOVA: F_2=27.05, P<0.001, Tukey's HSD corrected *post hoc* test: P=0.004, P<0.001).

Tracking performance

To quantify the consequences of wing damage for manoeuvrability during hovering flight, we used an artificial flower stimulus simultaneously moving at different temporal frequencies (Fig. 1B,D). To characterise the hawkmoth's flower tracking performance, we calculated the absolute displacement between hawkmoth and flower for the length of the stimulus. There was no significant difference in average displacement across treatments (Kruskall–Wallis test, χ^2_2=0.028, P=0.973; Fig. 5A, Table S1), nor in peak displacement (ANOVA: F_2=0.027, P=0.986; Fig. 5B, Table S1). Moreover, hawkmoth flight pathlengths, relative to the pathlength of the flower, did not differ between treatments (ANOVA: F_2=0.978, P=0.385; Fig. 5C, Table S1), neither was there a significant linear correlation of either of these measures with the wing length of the animals (Fig. 5D–F).

To analyse the flower tracking performance for the combined frequency response of the moth in detail, we extracted the gain and phase of the hawkmoth's response (Fig. 6A,B). We observed tracking responses with distinct gain and phase characteristics: a gain overshoot between 2 and 4 Hz, as well as a plateau of the gain between 6 and 11 Hz. This secondary plateau had a higher gain in the artificial damage group compared with the control and natural damage group with non-overlapping confidence intervals (Fig. 6A).

From the combination of gain and phase we calculated a tracking error metric (see Materials and Methods), to quantitatively compare the flower tracking performance of the different treatment groups (Fig. 6C). The average tracking error of the different treatment groups was very similar: it was low for frequencies below 1 Hz, and then rose to 1 at about 2.5 Hz. Correspondingly, the total tracking error in the lower frequency range, in which 95% of the power of flower movements is concentrated (Sponberg et al., 2015), did not differ significantly between treatment groups (ANOVA: F_2=2.03, P=0.145; Fig. 6D, Table S1), neither did it differ in the high frequency range 1.9–8.9 Hz (Kruskall–Wallis test, χ^2_2=5.06, P=0.078; Fig. 6E, Table S1). The total tracking error integrated over all temporal frequencies did not correlate with the relative forewing length (Pearson correlation coefficient r=0.01, P=0.941, n=34), or forewing area (Pearson correlation coefficient r=–0.02,

Journal of Experimental Biology (2021) 224, jeb236240. doi:10.1242/jeb.236240

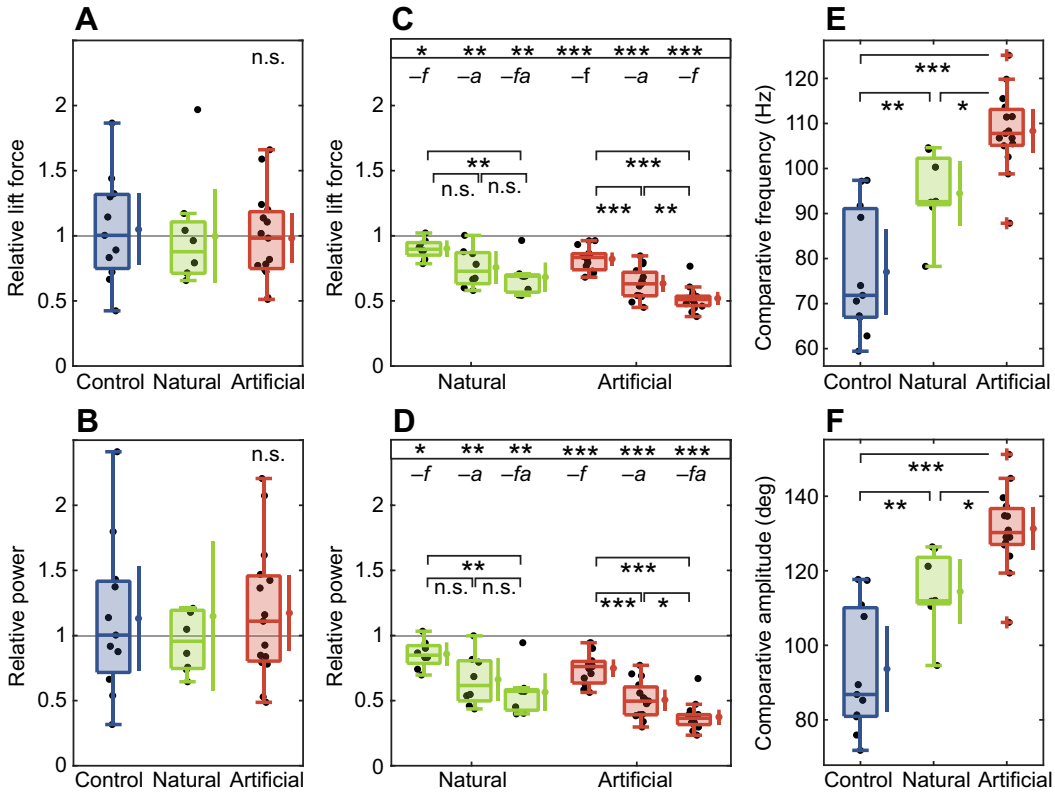

Fig. 4. Estimated lift generated, and mechanical power required for flapping. We calculated the lift force generated during hovering (A) for the three treatment groups, as well as the mechanical power (B) required for flapping, based on their wing shape, wing beat frequency and wing stroke amplitude in the wing stroke plane. Results were normalised relative to the median of the control group. We compared the estimated lift force (C) and mechanical power (D) within each treatment for three scenarios: with the measured wing beat amplitude (transformed to the stroke plane) and the median wing beat frequency of the control group (*–f*), with the measured frequency and median amplitude of the control group (*–a*) and with both median frequency and amplitude of the control (*–fa*). For each treatment, the resulting lift force and power predictions were normalised by the treatment predictions based on the measured parameters. Using the fixed median wing stroke amplitude of the control group, we calculated the wing beat frequency required to generate the same lift as with both the measured amplitude and frequency (E), and vice versa for the wing stroke amplitude (F). Statistical differences between groups are indicated as: ***P<0.001, **P<0.01, *P<0.05 (ANOVA with Tukey's HSD corrected *post hoc* test was performed after confirming normality of residuals; see Table S1; control: n=11; natural: n=8; artificial: n=15). In C and D, a Wilcoxon signed rank test was used to compare the median of each group with 1: ***P<0.001, **P<0.01, *P<0.05, n.s. P>0.05; see Table S2B. The coloured dot to the right of each boxplot shows the mean, and the bar indicates the 95% confidence interval.

P=0.921, n=34), and neither with absolute animal size (Pearson correlation coefficient r=−0.21, P=0.245, n=34). An error of 1, above which the animal would do equally well by staying stationary, was reached at the same frequency for all treatment groups, indicating that there was no significant difference in the temporal response of the different groups (ANOVA: F_2=3.12, P=0.407; Fig. 6F, Table S1).

DISCUSSION

Hummingbird hawkmoths use a combination of frequency and amplitude to compensate for wing damage

In our study on the effects of wing damage on flight performance in the hawkmoth *M. stellatarum* we observed significant effects of wing damage on the flight kinematics. Similarly to other studies previously performed on the hawkmoth *M. sexta* (Fernández et al., 2012, 2017), as well as on butterflies (Kingsolver, 1999) and bumblebees (Hedenström et al., 2001; Haas and Cartar, 2008), hummingbird hawkmoths increased their wing beat frequency when their wings were damaged (Fig. 2A). The wing beat frequency was increased proportionally to the amount of forewing area and length lost (Fig. 3). The increase in wing beat frequency in wing-damaged hummingbird hawkmoths was larger than in *M. sexta* (10% compared with less than 5%; Fernández et al., 2017), and larger in relative terms than the changes in wing beat frequency observed in bumblebees upon comparable extent of wing damage, though similar in absolute extent (Hedenström et al., 2001; Haas and Cartar, 2008). Thus, unlike previously thought (Fernández et al., 2017), our findings show that wing beat frequency can also be flexibly adjusted in insects with synchronous flight muscles, to a similar extent as in insects with asynchronous flight muscles.

Interestingly, we also observed a significant and substantial increase in wing beat amplitude in hawkmoths with damaged wings (Fig. 2B). A similar increase in wing beat amplitude has not been observed in any of the species so far studied –although there was a marginally significant increase in wing beat amplitude in *M. sexta* (Fernández et al., 2017). The increase in *M. stellatarum*, however, was much larger than in *M. sexta*, and reached about 30%, while in *M. sexta* it was only 5%. Together, our model results indicate that in *M. stellatarum*, the adjustments in wing beat kinematics are sufficient to compensate for the loss in lift force in the damage treatments, without a significant increase in mechanical power required to move the wings (Fig. 4).

Why, though, did hummingbird hawkmoths show a much more pronounced change in wing beat kinematics to compensate for a loss of wing area than their larger relative *M. sexta*? A striking difference in flight kinematics between *M. sexta* and *M. stellatarum* is their average wing beat frequency, and their overall difference in size

Journal of Experimental Biology (2021) 224, jeb236240. doi:10.1242/jeb.236240

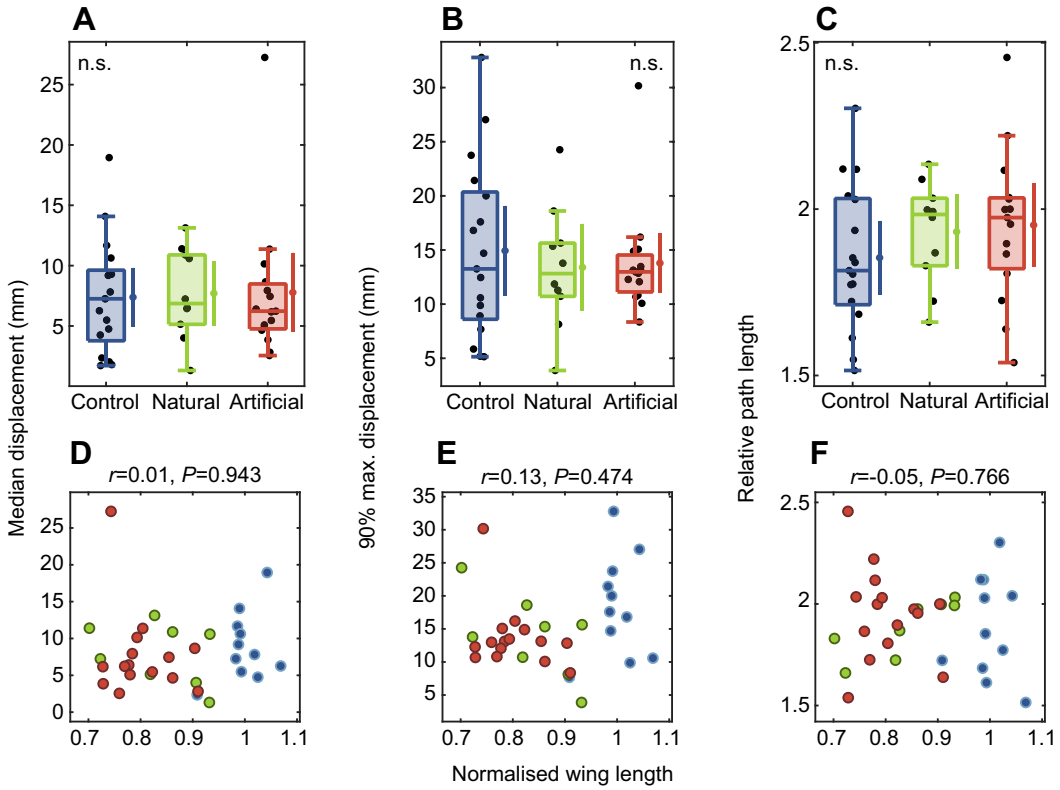

Fig. 5. Flower tracking performance in wing damaged hummingbird hawkmoths. Median displacement (A), 90% maximum displacement (B), measured at the Euclidian distance between the hawkmoth's thorax and flower nectary and flight path length (C) of the control, natural and artificial wing damage groups. Statistical differences between groups are indicated as: n.s. $P>0.05$ (ANOVA with Tukey's HSD corrected *post hoc* test performed after confirming the normality of residuals, Table S1, control: $n=17$; natural: $n=10$; artificial: $n=15$). (D–F) Linear correlation between normalised wing length median displacement (D), 90% maximum displacement (E) and flight path length (F). R indicates the strength of the linear correlation, and p the statistical significance of the Pearson correlation coefficient (control: $n=11$; natural: $n=8$; artificial: $n=15$). The coloured dot to the right of each boxplot shows the mean, and the bar indicates the 95% confidence interval.

(*M. sexta* has more than twice the wingspan of *M. stellatarum* and on average weighs 5 times as much; Henningsson and Bomphrey, 2013). However, the general shape of the wings across hawkmoths is very similar, suggesting similar hovering kinematics. Their wing loading and span efficiency have been shown to be similar (Henningsson and Bomphrey, 2013). Yet, this assessment was based on experiments performed on tethered individuals in a wind tunnel, so the results might differ from those for freely hovering individuals. Indeed, the wing beat frequency of freely hovering *M. stellatarum* is almost twice as high as that measured in tethered animals (76 Hz in Fig. 2 versus 48 Hz; Henningsson and Bomphrey, 2013). Thus, further kinematic studies investigating hovering flight in diverse hawkmoths will be necessary to understand the striking differences in wing beat kinematics following wing damage in these two hawkmoths species.

The high wing beat frequency of *M. stellatarum* might require a compensation strategy via wing beat amplitude

Why did we observe a much greater contribution of wing beat amplitude in lift force compensation than previously observed in other insects? Our modelling gives some indication for why *M. stellatarum* might use this strategy, rather than compensate almost entirely by adjusting wing beat frequency, as most other insects do. Based on our calculations, in order to compensate the reduction in lift force due to wing damage entirely by adjusting wing beat frequency, an average frequency of 93 Hz for the natural and 108 Hz for the artificial group would be required (Fig. 4E). However, such wing beat frequencies might exceed the range of synchronous flight muscles (Dudley, 2000; Syme, 2002), the muscle type possessed by hawkmoths. Indeed, none of the hawkmoths in our study (in any treatment group) reached even the more moderate wing beat frequency increase of 94 Hz required for the natural damage group (Fig. 2A). Since the wing beat frequency of intact *M. stellatarum* is already close to the upper limit for synchronous flight muscles, compensating lift force production entirely by wing beat frequency might not be an option for this hawkmoth species, and therefore a reason why we observed a larger contribution of wing beat amplitude to lift force compensation (Fig. 4C). The significant contribution of wing beat frequency, nevertheless, suggests that wing beat amplitude alone might not be sufficient to compensate the reduction in lift force upon wing damage. It is therefore likely that the required increase in wing beat amplitude (especially in the artificial damage case) might be outside biomechanical limits at the relatively high wing beat frequencies employed by *M. stellatarum*.

A potential beneficial side-effect of this compensation strategy, which relies heavily on increases in wing beat amplitude rather than frequency, is a reduction in the inertial power required to move the wings. While the aerodynamic power (Fig. 4B) scales similarly for changes in wing beat frequency and amplitude, inertial power scales with the square of stroke amplitude and the cube of wing beat frequency (Willmott and Ellington, 1997a). Inertial power is often not considered as a cost, because it is assumed that minimal power is required for the inertial acceleration of the wings because of energy storage and return. However, it has been shown that the inertial power, while significantly reduced, is not perfectly compensated by elastic elements (Gau et al., 2019). Thus, the amplitude-based

Journal of Experimental Biology (2021) 224, jeb236240. doi:10.1242/jeb.236240

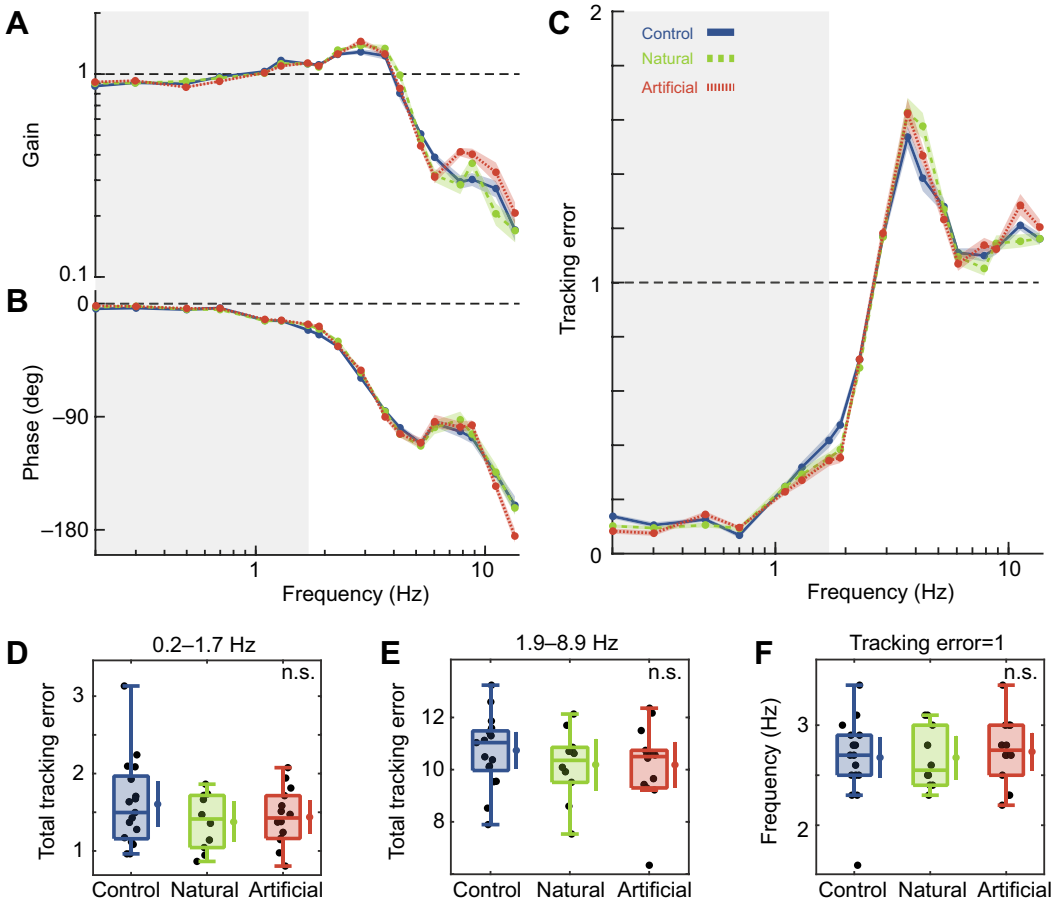

Fig. 6. Flower tracking performance of the treatment groups at different temporal frequencies. Gain (A), phase (B) and tracking error (C) of the control, natural and artificial wing damage groups. Curves show the means and 95% confidence intervals computed in the complex plane. The total tracking error for each group over a low (D) and a high (E) temporal frequency range. (F) The temporal frequency at which the tracking error approached 1 for each treatment group. Statistical analysis was performed using a Kruskal–Wallis test (D,F) and an ANOVA with Tukey's HSD corrected *post hoc* test (E) after testing the normality of the residuals. n.s. $P>0.05$ (control: $n=17$; natural: $n=10$; artificial: $n=15$; see Table S1). The grey areas represent the lower temporal range of tracking frequencies analysed in A. The coloured dot to the right of each boxplot shows the data mean, and the bar indicates the 95% confidence interval.

strategy of *M. stellatarum* should be beneficial from an inertial power point of view, and equally good as far as aerodynamic power is concerned. This raises the question, however, why all other insect species investigated so far showed a frequency-based compensation strategy. One important aspect speaking against an amplitude-based compensation strategy, in particular for insects with asynchronous flight muscles, is that modulations of wing beat amplitude are required for steering. Thus, increasing the average wing beat amplitude proportionally leaves less room for amplitude changes, which might therefore affect manoeuvrability in these insects. It will therefore be interesting to investigate in the future whether insects with synchronous and asynchronous flight muscles apply different strategies when compensating for wing damage, and what role other factors, such as body and wing size, might play.

Flower tracking manoeuvrability is not compromised by natural or artificial wing damage

While the effects of wing damage on flight kinematics show some common trends across the different species of insects studied previously, it is less well understood what effects wing damage has on the manoeuvrability of fast flying insects, and thus ultimately on their foraging and predator avoidance success. In our setup, we studied the effects of wing damage on the manoeuvrability of hawkmoths in a task which is very similar to their natural foraging paradigm. Moreover, we tested the effect of wing damage quantitatively over a range of temporal frequencies, which allowed us to assess whether wing damage affected particular temporal aspects of the hawkmoth's flower tracking ability, as does alteration of their sensory input (Sponberg et al., 2015; Roth et al., 2016; Stöckl et al., 2017; Dahake et al., 2018). However, we did not find any significant impairment of the tracking performance in wing-damaged hawkmoths (Figs 6 and 7), and no significant difference in tracking error within the frequency range in which flowers naturally move (Sponberg et al., 2015; Fig. 6D), nor indeed at any frequency across the entire range. We did, however, observe an interesting difference between the three treatment groups in the shape of their tracking response, in particular in the tracking gain: individuals with artificial wing damage had higher tracking gains for frequencies ranging from 4.5 to 12 Hz (Fig. 6A). The particular shape of the frequency response (Fig. 6A,B) is a representation of the full sensory to motor dynamics of the hovering moth. These differences could therefore arise either from changes in flight kinematics affecting the mechanics of flight, or from context-dependent changes in neural processing due to damage.

The results of a previous study on the kinematics of lateral manoeuvres in hawkmoths suggests that wing damage, and the changes in flight kinematics induced by wing damage, might indeed affect lateral manoeuvres (Greeter and Hedrick, 2016): the hawkmoth *M. sexta* uses asymmetries between the left and right

wing stroke pitch angle, and to a lesser degree of the wing stroke amplitude, to initiate lateral movements of the type we studied here in *M. stellatarum* via roll manoeuvres. Moreover, *M. sexta* flapped with greater amplitudes during sideslips to increase their net manoeuvre force. The increased wing beat amplitude in wing-damaged *M. stellatarum* should therefore have reduced the operational flexibility of the moths to vary wing their stroke amplitude during manoeuvres or to increase it during sideslip. Furthermore, alternative strategies based on flapping frequency changes would also have been jeopardised by approaching the upper limit of wing beat frequency in the damaged individuals. The fact that we did not observe any effects of wing damage on flower tracking performance might therefore indicate that *M. stellatarum* relies on a manoeuvring strategy based on wing pitch variations rather than amplitude variations, which would also be capable of supporting these lateral manoeuvres (Greeter and Hedrick, 2016). Future studies of the wing pitch angles of intact and wing-damaged individuals resolved at wing-beat precision while the hawkmoths are tracking flowers could reveal such a change in strategy.

Even though the changes in flight performance we observed between control and damage groups (Fig. 6A,B) did not affect overall tracking error, they might still reflect functional differences in the control and damaged conditions. Previously, changes in gain within a species were observed upon altered sensory input necessary for flight control, for example when the animals had reduced luminance (Sponberg et al., 2015; Stöckl et al., 2017), conflicting mechanosensory and visual cues (Roth et al., 2016) or were deprived of fast sensory input about the animal's own movements (Dahake et al., 2018). Without the latter form of feedback, the animals could not track fast movements of the flower, and the gain in the high frequency range decreased compared with the controls. Interestingly, with wing damage, the gain increased in the high frequency range compared with the control group, suggesting that wing damaged animals performed coordinated flight manoeuvres with larger amplitudes within this range. A potential explanation for this observation might be the increased wing beat frequency observed in the wing damage groups. It might allow the animals to perform more accurate flight manoeuvres even at higher frequencies because the necessary adjustments of the hawkmoth's position could be performed faster. While the effects were relatively small and manifested only outside the range the animals usually experience, it shows that manipulating the wing anatomy could also be used to artificially change different aspects of wing beat kinematics and study their role in fine-scale flight control.

Overall, our findings suggest that intact wings are not crucial for the precise control of lateral flight manoeuvres, which hawkmoths perform tracking flowers within their natural movement range (Sponberg et al., 2015). This is in line with results from foraging butterflies and bumblebees, which likewise showed no significant alterations in flight or foraging performance (Kingsolver, 1999; Haas and Cartar, 2008). The system identification approach we used on the sum-of-sines stimulus allowed us to extend this conclusion over the full temporal frequency response of the moth's behaviour. One explanation that might reconcile our results and previous findings from dragonflies, which showed a strong impairment in flight performance upon wing wear (Combes et al., 2010) is the direction in which flight manoeuvres were executed. In our experiments, the insects were conducting horizontal flight manoeuvres, while in dragonflies the vertical acceleration was impaired, and animals often perform vertical manoeuvres during prey capture, which showed a reduction in success upon wing damage (Combes et al., 2010). One might therefore hypothesise that wing damage affects some flight manoeuvres stronger than others, and that intact wings might be particularly important for fast vertical manoeuvres.

Conclusion

Taken together, our results show that hummingbird hawkmoths compensate for a loss in wing area by increases in wing beat frequency and amplitude, and track moving flowers without a performance impairment. This impressive tolerance to wing damage might be a testament to the immense importance that fast steering has for these animals: not only do they feed exclusively on the wing, and very rarely land on flowers, they also lay their eggs on their hostplant while hovering in front of the plants (Stöckl and Kelber, 2019). Moreover, since hummingbird hawkmoths hibernate as adults, resulting in lifespans of several months (Pittaway, 1993), optimising their flight abilities to tolerate wing damage might be paramount for the fitness of these insects. Their strategy to compensate for the loss in wing area both by an increase in wing stroke amplitude and wing beat frequency, suggests that multiple kinematics strategies could be utilized to compensate for wing damage in different insect species. It opens up future study directions to better understand which kinematic, aerodynamic and behavioural aspects govern the strategies of insects to compensate for wing damage while retaining optimal manoeuvrability.

Acknowledgements

We thank Merry and Leigh Foster for help with capturing the parental moths in France, and Marie Dacke for allowing us to use her high-speed cameras. We thank Usama Bin Sikandar for help with analysis.

Competing interests

The authors declare no competing or financial interests.

Funding

This work was supported by a National Science Foundation Postdoctoral Research Fellowship in Biology (DBI-1812107) to B.A., an NSF Faculty Early Career Development Award (1554790) to S.S. and grants from the Swedish Research Council (2016-04014) and the Air Force Office of Scientific Research (FA9550-12-1-0237) to E.W.

Author contributions

Conceptualization: K.K., A.L.S.; Methodology: S.S., A.L.S.; Validation: K.K., A.L.S.; Formal analysis: K.K., B.A., S.S., A.L.S.; Investigation: K.K.; Resources: E.J.W., S.S., A.L.S.; Data curation: K.K., A.L.S.; Writing - original draft: A.L.S.; Writing - review & editing: K.K., B.A., E.J.W., S.S., A.L.S.; Visualization: A.L.S.; Supervision: S.S., A.L.S.; Project administration: A.L.S.; Funding acquisition: B.A., E.J.W., S.S.

Data availability

Data supporting the presented results is available in Figshare at: https://figshare.com/s/73ad11df08567ea76d9d. The custom-written MATLAB code used to analyse the data and prepare the figures is available from the corresponding author upon request.

Supplementary information

Supplementary information available online at
https://jeb.biologists.org/lookup/doi/10.1242/jeb.236240.supplemental

References

Cartar, R. V. (1992). Morphological senescence and longevity: An experiment relating wing wear and life span in foraging wild bumble bees. *J. Anim. Ecol.* **61**, 225-231. doi:10.2307/5525

Combes, S. A., Crall, J. D. and Mukherjee, S. (2010). Dynamics of animal movement in an ecological context: dragonfly wing damage reduces flight performance and predation success. *Biol. Lett.* **6**, 426-429. doi:10.1098/rsbl.2009.0915

Cowan, N. J., Ankarali, M. M., Dyhr, J. P., Madhav, M. S., Roth, E., Sefati, S., Sponberg, S., Stamper, S. A., Fortune, E. S. and Daniel, T. L. (2014). Feedback control as a framework for understanding tradeoffs in biology. *Integr. Comp. Biol.* **54**, 223-237. doi:10.1093/icb/icu050

Dahake, A., Stöckl, A. L., Foster, J. J., Sane, S. P. and Kelber, A. (2018). The roles of vision and antennal mechanoreception in hawkmoth flight control. *eLife* **7**, e37606. doi:10.7554/eLife.37606

Dakin, R., Segre, P. S., Straw, A. D. and Altshuler, D. L. (2018). Morphology, muscle capacity, skill, and maneuvering ability in hummingbirds. *Science* **359**, 653-657. doi:10.1126/science.aao7104

Dudley, R. (2000). *The Biomechanics of Insect Flight: Form, Function, Evolution*. Princeton University Press.

Ellington, C. P. (1984a). The aerodynamics of hovering insect flight. II. morphological parameters. *Philos. Trans. R. Soc. Lond. B Biol. Sci.* **305**, 17-40. doi:10.1098/rstb.1984.0050

Ellington, C. P. (1984b). The aerodynamics of hovering insect flight. III. kinematics. *Philos. Trans. R. Soc. Lond. B Biol. Sci.* **305**, 41-78. doi:10.1098/rstb.1984.0051

Ellington, C. P. (1984c). The aerodynamics of hovering insect flight. VI. lift and power requirements. *Philos. Trans. R. Soc. Lond. B Biol. Sci.* **305**, 145-181. doi:10.1098/rstb.1984.0054

Ellington, C. P. and Lighthill, M. J. (1984a). The aerodynamics of hovering insect flight. I. the quasi-steady analysis. *Philos. Trans. R. Soc. Lond. B Biol. Sci.* **305**, 1-15. doi:10.1098/rstb.1984.0049

Ellington, C. P. and Lighthill, M. J. (1984b). The aerodynamics of hovering insect flight. IV. aerodynamic mechanisms. *Philos. Trans. R. Soc. Lond. B Biol. Sci.* **305**, 79-113. doi:10.1098/rstb.1984.0052

Farina, W. M., Varjú, D. and Zhou, Y. (1994). The regulation of distance to dummy flowers during hovering flight in the hawk moth *Macroglossum stellatarum*. *J. Comp. Physiol. A* **174**, 239-247. doi:10.1007/BF00193790

Fernández, M. J., Driver, M. E. and Hedrick, T. L. (2017). Asymmetry costs: effects of wing damage on hovering flight performance in the hawkmoth *Manduca sexta*. *J. Exp. Biol.* **220**, 3649-3656. doi:10.1242/jeb.153494

Fernández, M. J., Springthorpe, D. and Hedrick, T. L. (2012). Neuromuscular and biomechanical compensation for wing asymmetry in insect hovering flight. *J. Exp. Biol.* **215**, 3631-3638. doi:10.1242/jeb.073627

Gau, J., Gravish, N. and Sponberg, S. (2019). Indirect actuation reduces flight power requirements in *Manduca sexta* via elastic energy exchange. *J. R. Soc. Interface* **16**, 20190543. doi:10.1098/rsif.2019.0543

Greeter, J. S. M. and Hedrick, T. L. (2016). Direct lateral maneuvers in hawkmoths. *Biol. open* **5**, 72-82. doi:10.1242/bio.012922

Haas, C. A. and Cartar, R. V. (2008). Robust flight performance of bumble bees with artificially induced wing wear. *Can. J. Zool.* **86**, 668-675. doi:10.1139/Z08-034

Hedenström, A., Ellington, C. P. and Wolf, T. J. (2001). Wing wear, aerodynamics and flight energetics in bumblebees (*Bombus terrestris*): an experimental study. *Funct. Ecol.* **15**, 417-422. doi:10.1046/j.0269-8463.2001.00531.x

Hedrick, T. L. (2008). Software techniques for two- and three-dimensional kinematic measurements of biological and biomimetic systems. *Bioinspir. Biomim.* **3**, 034001. doi:10.1088/1748-3182/3/3/034001

Hedrick, T. L., Cheng, B. and Deng, X. (2009). Wingbeat time and the scaling of passive rotational damping in flapping flight. *Science* **324**, 252-255. doi:10.1126/science.1168431

Henningsson, P. and Bomphrey, R. J. (2013). Span efficiency in hawkmoths. *J. R. Soc. Interface* **10**, 20130099. doi:10.1098/rsif.2013.0099

Kingsolver, J. G. (1999). Experimental analyses of wing size, flight, and survival in the western white butterfly. *Evolution* **53**, 1479-1490. doi:10.1111/j.1558-5646.1999.tb05412.x

Mountcastle, A. M., Alexander, T. M., Switzer, C. M. and Combes, S. A. (2016). Wing wear reduces bumblebee flight performance in a dynamic obstacle course. *Biol. Lett.* **12**, 20160294. doi:10.1098/rsbl.2016.0294

Pittaway, A. (1993). *The Hawkmoths of the Western Palearctic*. Colchester, UK: Harley Books.

Roth, E., Zhuang, K., Stamper, S. A., Fortune, E. S. and Cowan, N. J. (2011). Stimulus predictability mediates a switch in locomotor smooth pursuit performance for *Eigenmannia virescens*. *J. Exp. Biol.* **214**, 1170-1180. doi:10.1242/jeb.048124

Roth, E., Hall, R. W., Daniel, T. L. and Sponberg, S. (2016). Integration of parallel mechanosensory and visual pathways resolved through sensory conflict. *Proc. Natl Acad. Sci. USA* **113**, 12832-12837. doi:10.1073/pnas.1522419113

Roth, E., Sponberg, S. and Cowan, N. J. (2014). A comparative approach to closed-loop computation. *Curr. Opin. Neurobiol.* **25**, 54-62. doi:10.1016/j.conb.2013.11.005

Schindelin, J., Arganda-Carreras, I., Frise, E., Kaynig, V., Longair, M., Pietzsch, T., Preibisch, S., Rueden, C., Saalfeld, S., Schmid, B. et al. (2012). Fiji: an open-source platform for biological-image analysis. *Nat. Methods* **9**, 676-682. doi:10.1038/nmeth.2019

Sponberg, S., Dyhr, J. P., Hall, R. W., Daniel, T. L. (2015). Insect flight. luminance-dependent visual processing enables moth flight in low light. *Science* **348**, 1245-1248. doi:10.1126/science.aaa3042

Sprayberry, J. D. H. and Daniel, T. L. (2007). Flower tracking in hawkmoths: behavior and energetics. *J. Exp. Biol.* **210**, 37-45. doi:10.1242/jeb.02616

Stöckl, A. L. and Kelber, A. (2019). Fuelling on the wing: sensory ecology of hawkmoth foraging. *J. Comp. Physiol. A Neuroethol. Sens. Neural. Behav. Physiol.* **205**, 399-413. doi:10.1007/s00359-019-01328-2

Stöckl, A. L., Kihlström, K., Chandler, S. and Sponberg, S. (2017). Comparative system identification of flower tracking performance in three hawkmoth species reveals adaptations for dim light vision. *Philos. Trans. R. Soc. Lond. B Biol. Sci.* **372**, 20160078. doi:10.1098/rstb.2016.0078

Syme, D. A. (2002). How to build fast muscles: Synchronous and asynchronous designs. *Integr. Comp. Biol.* **42**, 762-770. doi:10.1093/icb/42.4.762

Usherwood, J. R. and Ellington, C. P. (2002). The aerodynamics of revolving wings ii. Propeller force coefficients from mayfly to quail. *J. Exp. Biol.* **205**, 1565-1576.

Voigt, C. C. (2013). Bat flight with bad wings: is flight metabolism affected by damaged wings? *J. Exp. Biol.* **216**, 1516-1521. doi:10.1242/jeb.079509

Warton, D. I., Wright, I. J., Falster, D. S. and Westoby, M. (2006). Bivariate line-fitting methods for allometry. *Biol. Rev. Camb. Philos. Soc.* **81**, 259-291. doi:10.1017/S1464793106007007

Willmott, A. P. and Ellington, C. P. (1997a). The mechanics of flight in the hawkmoth *Manduca sexta*. I. kinematics of hovering and forward flight. *J. Exp. Biol.* **200**, 2705-2722.

Willmott, A. P. and Ellington, C. P. (1997b). The mechanics of flight in the hawkmoth *Manduca sexta*. II. aerodynamic consequences of kinematic and morphological variation. *J. Exp. Biol.* **200**, 2723-2745.

Supplementary Figures

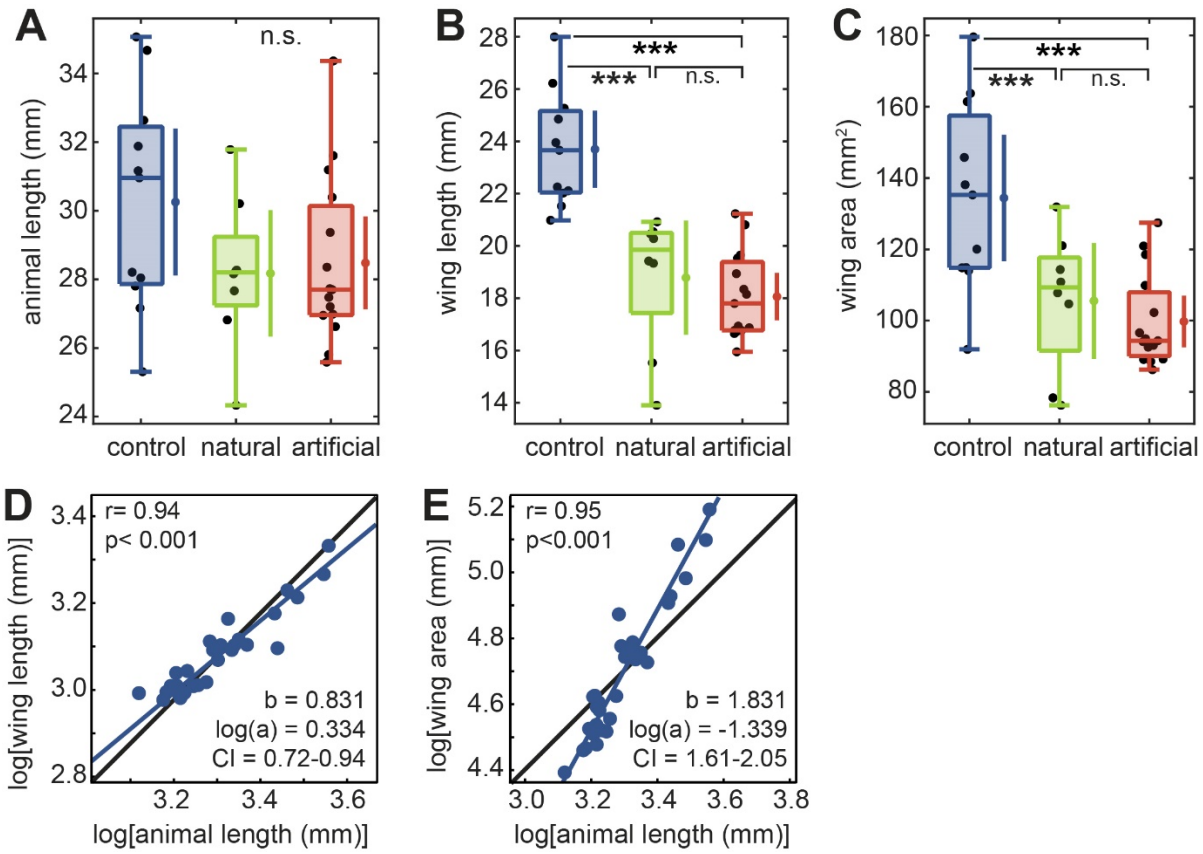

Figure S1. Body and wing anatomy of the different treatment groups. A Absolute length of the animals, measured from their anterior to posterior extent, **B** absolute length of the forewings from the wing base to the tip and **C** absolute wing area. Statistical differences between groups are indicated as: *** $p < 0.001$, ** $p < 0.01$, * $p < 0.05$, n.s. $p > 0.05$ (ANOVA with Tukey's HSD corrected post-hoc test was performed after confirming normality of residuals, see Table S1, *control*: n=11, *natural*: n=8, *artificial*: n=15). The dots next to each boxplot show the data's mean, and the lines around them the 95% confidence intervals around the mean. **D, E** Linear correlation between animal length and wing length (**D**) and wing area (**E**) on a logarithmic scale. r indicates the strength of the linear correlation, and p the statistical significance of the Pearson correlation coefficient, n=31. The allometric relationship was calculated using reduced major axis regression, where b is the exponential scaling exponent and log(a) is the log-transformed scaling constant of the allometric relationship. The 95% confidence interval of the slope is given by CI.

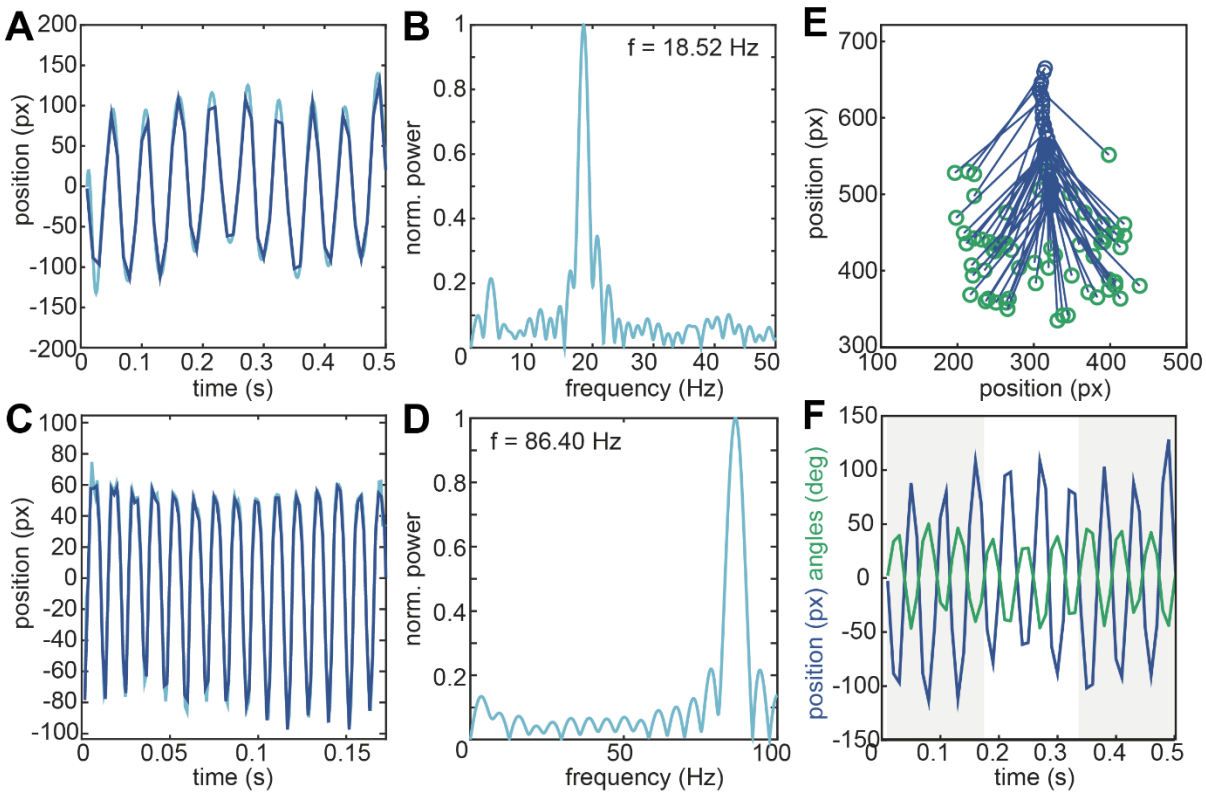

Figure S2. Wing beat frequency and amplitude measurements. A The wing beat of the animals in this study was measured by tracking the position of the tip of their wing for at least 100 frames. **B** The position data was then Fourier transformed and the wing beat frequency extracted as the peak in the power spectrum. Since the video frame rate of 100 fps resulted in a Nyquist frequency lower than the true wing beat frequency, the calculated frequency was subtracted from 100 Hz to obtain the real wing beat frequency. **C** The true wing beat frequency was measured in selected individuals using a frame rate of 600 fps. **D** Using this frame rate, the wing beat frequency was confirmed to range around 80 Hz, and thus exceed the Nyquist frequency at 100 fps. **E,F** Wing beat amplitude was calculated as the maximum angle between the most extreme wing positions measured over 5 consecutive wing beats, to avoid underestimating the real amplitude due to the temporal undersampling of the wing beat. **F** The wing tip position is shown in blue, the angles between the wing tip and body axis are shown in green.

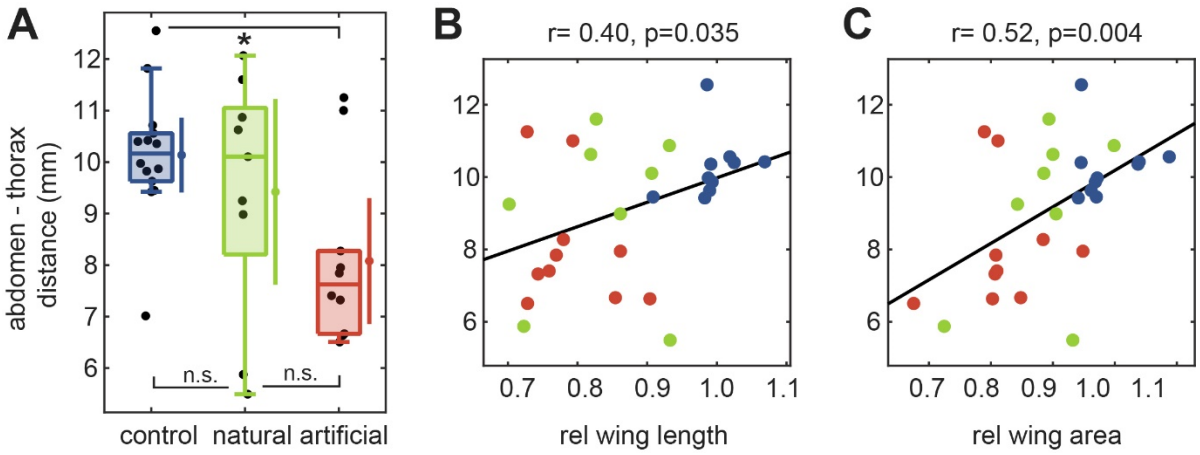

Figure S3. Body pitch angle of the different treatment groups. A We indirectly measured the pitch angle of the hawkmoth's body by comparing the distance between the thorax and the distal tip of the abdomen in the dorsal camera view while each hawkmoth was hovering at the artificial flower. Black dots denote average thorax – abdomen distance for each hawkmoth. Statistical differences between groups are indicated as: *** $p < 0.001$, ** $p < 0.01$, * $p < 0.05$, n.s. $p > 0.05$ (ANOVA with Tukey's HSD corrected post-hoc test was performed after confirming normality of residuals, Table S1, *control*: n=14, *natural*: n=9, *artificial*: n=10). **B,C** We furthermore tested for correlations between the thorax – abdomen distance and the relative wing length and the relative wing area. The strength of the linear correlation is given by r, and the statistical significance of the Pearson correlation coefficient by p (*control*: n=11, *natural*: n=8, *artificial*: n=10). The dots next to each boxplot show the data's mean, and the lines around them the 95% confidence intervals around the mean.

Supplementary Tables

Table S1 Statistical results of comparisons of population means / medians between the three damage conditions, using an ANOVA (df = 2) with Tukey's HSD corrected post-hoc test when normality of the residuals was confirmed (F-statistic), or a Kruskall-Wallis test (df = 2) with Tukey's HSD corrected post-hoc test (X^2-statistic) when it was not. Tested parameters are given in bold letters in the top row of each block of tests, the second row indicates the figures that show the corresponding data, and each last row per block indicates the number of individuals in each condition.

		animal length	**wing length**	**wing area**	**rel. wing length**	**rel. wing area**	**wing beat frequency**	**wing beat amplitude**	**angular velocity**	**thorax – abdomen distance**
		Fig.1 - S1A	Fig.1 - S1B	Fig.1 - S1C	Fig.1E	Fig.1F	Fig.2A	Fig.2B	Fig.2C	Fig.2 – S2A
test statistic, p-value		1.895 (F), 0.167	25.27 (F), <0.001	10.46 (F), <0.001	34.04 (F), <0.001	18.96 (F), <0.001	13.09(F), <0.001	25.35 (F), <0.001	35.59 (F), <0.001	4.10 (F), 0.0267
post-hoc p-values for:										
control	natural	0.228	<0.001	0.010	<0.001	0.070	0.070	0.013	0.004	0.607
control	artificial	0.228	<0.001	<0.001	<0.001	<0.001	<0.001	<0.001	<0.001	0.021
natural	artificial	0.963	0.707	0.781	0.381	0.083	0.083	0.007	<0.001	0.229
nr of individuals		11 8 15	11 8 15	11 8 15	11 8 15	11 8 15	17 10 15	17 10 15	17 10 15	14 9 10

		rel. lift force	**rel. mech. power**	**freq. – fix. ampl.**	**ampl. – fix. freq.**
		Fig.4A	Fig.4B	Fig.4E	Fig.4F
test statistic, p-value		0.103 (F), 0.903	0.016 (F), 0.984	27.05(F), <0.001	27.05 (F), <0.001
post-hoc p-values for:					
control	natural	0.953	0.998	0.004	0.004
control	artificial	0.897	0.983	<0.001	<0.001
natural	artificial	0.996	0.995	0.016	0.016
nr of individuals		11 8 15	11 8 15	11 8 15	11 8 15

		median displacement	**90% max. displacement**	**path length**	**total error**	**error 0.2 - 1.7 Hz**	**error 1.9 - 8.9 Hz**	**error = 1**
		Fig.5A	Fig.5B	Fig.5C		Fig.5D	Fig.5E	Fig.6F
test statistic, p-value		0.028 (X^2), 0.973	0.027 (F), 0.986	0.978 (F), 0.385	2.92 (X^2), 0.233	2.03 (F), 0.145	5.06 (X^2), 0.078	3.12 (F), 0.407
post-hoc p-values for:								
control	natural	0.986	0.989	0.617	0.238	0.135	0.225	0.691
control	artificial	0.973	0.989	0.386	0.489	0.403	0.087	0.385
natural	artificial	0.999	0.999	0.969	0.931	0.784	0.911	0.886
nr of individuals		17 10 15	17 10 15	17 10 15	17 10 15	17 10 15	17 10 15	17 10 15

Table S2 A Comparison of population medians of the estimated normalised lift force and normalised mechanical power generated with measured wing beat amplitude and the median wing beat frequency of the control group (*-f*), with the measured frequency and the median amplitude of the control group (*-a*) and with both median frequency and amplitude of the control (*-fa*) (shown in Fig. 5C,D) within each damage condition. The results of an ANOVA (df = 2) with Tukey's HSD corrected post-hoc test where normality of residuals could be confirmed, for all others conditions a Kruskall-Wallis test with Tukey's HSD corrected post-hoc test was performed. The last row gives the number of individuals in each condition. **B** Comparison of population medians of the estimated normalised lift force generated during hovering and the normalised mechanical power required for flapping versus 1 (shown in Fig. 5C,D) across damage conditions. The number of individuals in each condition are the same as in **A**. The results of a Wilcoxon signed rank test are shown, with the same sample sizes as given in **A**, and df = 7 the natural and df = 14 for the artificial condition.

A

			natural			artificial		
lift force	test statistic, p-value		6.9 (F), 0.005			36.3 (F), <0.001		
	post-hoc p-values for:							
	-f	**-a**	0.065			<0.001		
	-f	**-fa**	0.004			<0.001		
	-a	**-fa**	0.435			0.007		
power	test statistic, p-value		6.7 (F), 0.006			36.0 (F), <0.001		
	post-hoc p-values for:							
	-f	**-a**	0.066			<0.001		
	-f	**-fa**	0.005			<0.001		
	-a	**-fa**	0.454			0.013		
nr of individuals			**11**	**8**	**15**	**11**	**8**	**15**

B

signed rank, p-value		natural		artificial	
lift	**-f**	36	0.016	0	<0.001
	-a	37	0.008	0	<0.001
	-fa	40	0.008	0	<0.001
power	**-f**	37	0.016	0	<0.001
	-a	37	0.008	0	<0.001
	-fa	41	0.008	0	<0.001